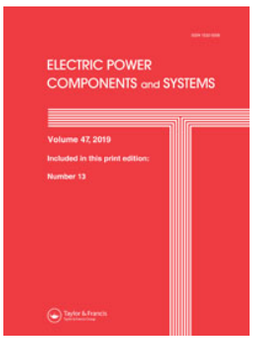

Taylor & Francis
Taylor & Francis Group

Electric Power Components and Systems

ISSN: 1532-5008 (Print) 1532-5016 (Online) Journal homepage: https://www.tandfonline.com/loi/uemp20

Multi-Resonant Indirect Digital Current Control Technique for Single-Phase Shunt Active Power Filters

Mohammad-Sadegh Karbasforooshan & Mohammad Monfared

To cite this article: Mohammad-Sadegh Karbasforooshan & Mohammad Monfared (2019) Multi-Resonant Indirect Digital Current Control Technique for Single-Phase Shunt Active Power Filters, Electric Power Components and Systems, 47:13, 1196-1202

To link to this article: https://doi.org/10.1080/15325008.2019.1627611

Published online: 26 Nov 2019.

Electric Power Components and Systems, 47(13): 1196–1202, 2019

ISSN: 1532-5008 print / 1532-5016 online
DOI: 10.1080/15325008.2019.1627611

Multi-Resonant Indirect Digital Current Control Technique for Single-Phase Shunt Active Power Filters

Mohammad-Sadegh Karbasforooshan and Mohammad Monfared
Department of Electrical Engineering, Faculty of Engineering, Ferdowsi University of Mashhad, Mashhad, Iran

CONTENTS

Abstract—This article proposes multi-resonant indirect digital current control technique for single-phase shunt active power filters. The main advantages of the suggested technique are simplicity, fast dynamics, low computational burden, and low current ripple. A straightforward design technique in the frequency domain is proposed to properly decide the controller gains and study its performance. Then, the digital implementation of the proposed control algorithm is presented, which lets implement it on a mid-range digital signal controller. Simulation and experimental results on a prototype system are reported to demonstrate the effectiveness of the proposed control system.

1. INTRODUCTION

Active power filters (APFs) have been introduced to alleviate the effects of grid current harmonics caused by nonlinear loads on the utility grid. These loads, which are rapidly growing, draw harmonic currents from the grid and distort the voltage and cause many other problems. The APFs can be used in shunt or series structure with the grid to compensate the harmonic currents and prevent the voltage from being distorted. Up to now, many different control techniques for the single-phase shunt APFs have been suggested. From these, one can point to the discrete Fourier transform (DFT) and its derivatives [1–3], instantaneous active and reactive power theory (PQ theory) and its derivatives [4–6], synchronous reference frame (SRF) method [7–9], repetitive control [10–11], sliding mode, H_∞ and nonlinear controls [12–15], neural network and fuzzy techniques and etc. [16–21]. These techniques have the common advantages such as precise detection of the fundamental and harmonic components, fast dynamic response, and selective harmonic compensation. But, complexity, high computational burden and low switching frequency (high current ripple) may be some limitations.

Keywords: indirect control, single-phase shunt active power filter, digital implementation, multi-resonant controller, proportional current controller, DC-link voltage controller, bandwidth frequency, harmonic compensation, fast dynamics, low computational burden

Received 7 June 2018; accepted 18 May 2019

Address correspondence to Mohammad Monfared, Department of Electrical Engineering, Faculty of Engineering, Ferdowsi University of Mashhad, Mashhad, Iran. E-mail: m.monfared@um.ac.ir

Color versions of one or more of the figures in the article can be found online at www.tandfonline.com/uemp.

This article proposes an indirect current control technique for the single-phase shunt APFs. This technique benefits from some advantages of simplicity, fast dynamic response, low computational burden. In the next sections, first the proposed technique is introduced and then the design details with digital implementation are discussed. Simulation and experimental results are presented, which confirm the proper operation of the proposed technique.

2. INDIRECT CURRENT CONTROL OF SINGLE-PHASE SHUNT ACTIVE POWER FILTERS

2.1. System Model and Indirect Current Control

Figure 1 shows the structure of a single-phase shunt active power filter. This structure consists of an inductor, a capacitor and four power semiconductor switches. The Kirchhoff's current law in the point of common coupling (PCC) is

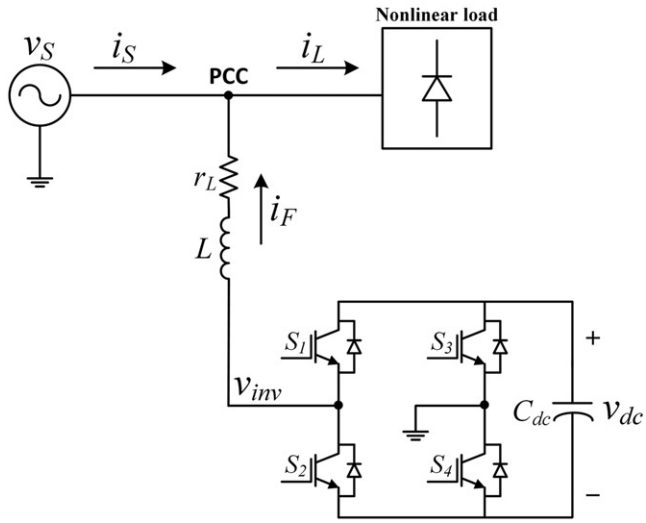

FIGURE 1. Single-phase shunt active power filter.

$$i_S = i_L - i_F \tag{1}$$

where i_S, i_L, i_F are source, load, and filter currents, respectively. The inverter output voltage is

$$v_{inv} = r_L i_F + L\frac{di_F}{dt} + v_S \tag{2}$$

This equation can be rewritten as

$$\left(L\frac{d}{dt} + r_L\right) i_F = v_{inv} - v_S \tag{3}$$

By applying Laplace operator to (3), one has

$$I_F(s) = \frac{1}{Ls + r_L}\left(V_{inv}(s) - V_S(s)\right) \tag{4}$$

Figure 2 shows the block-diagram of the proposed indirect current control for the single-phase shunt active power filters. This technique works with two voltage sensors and only one current sensor. The amplitude of the grid reference current is calculated by passing the difference of sensed DC-link voltage and its reference value through a proportional integral (PI) controller. The phase of the grid voltage, i.e. $\sin(\omega t)$, is easily obtained by dividing the sensed grid voltage by the voltage amplitude (the amplitude is not necessarily exact). By multiplying the amplitude and the phase of the grid reference current and by having a simple proportional gain, the final control signal to be compared with a carrier, is generated. Also, it is proposed to use a network of resonant controllers in parallel with the proportional controller to highly attenuate the specific harmonics of interest.

2.2. Proportional Current Controller Design

In order to design proportional current controller, the transfer function of the filter current loop should be obtained. Therefore, we have

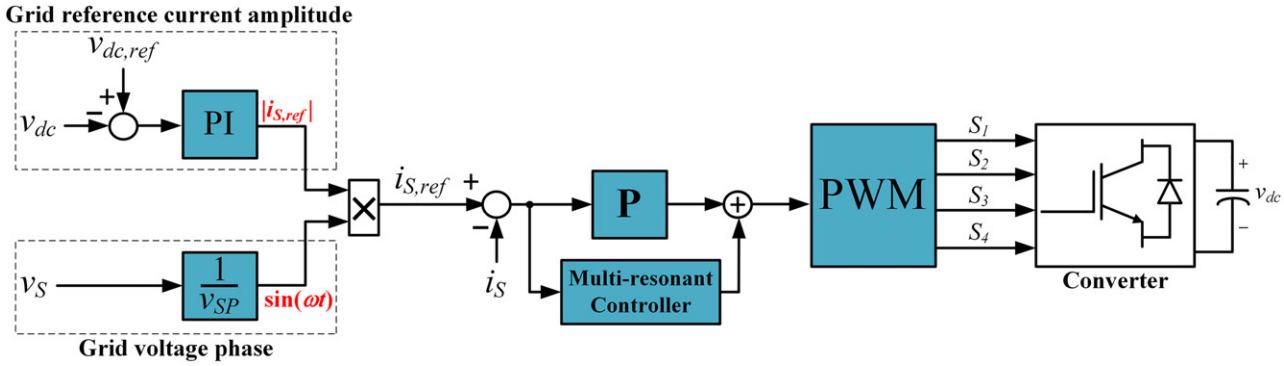

FIGURE 2. Proposed controller for single-phase shunt active power filters.

$$G_I(s) = \frac{I_F(s)}{I_{F,ref}(s)} = \frac{P}{Ls + (r_L + P)} \tag{5}$$

By considering −3dB attenuation of (5) at the desired current bandwidth frequency, one has

$$\frac{P^2}{(r_L + P)^2 + (L\omega_{bi})^2} = \frac{1}{2} \tag{6}$$

Therefore, the proportional current controller is obtained as

$$P = r_L + \sqrt{2r_L^2 + L^2\omega_{bi}^2} \tag{7}$$

Because the load current has a negligible dynamic, this proportional gain can be used in the source current loop (in Figure 2), also. The current control bandwidth of the active power filter should be chosen enough higher than the largest harmonic frequency, which is decided to be effectively compensated, in order to provide enough control action (gain) up to that harmonic frequency. Also, the bandwidth must be chosen adequately less than the switching frequency to prevent the switching harmonics (noises) to affect the current control performance. Therefore, the current control bandwidth selection is a tradeoff between the reference tracking and the attenuation of the switching frequency components. So, the current control bandwidth frequency is selected in the range of one-fifth to one-third of the switching frequency.

2.3. DC-Link Voltage Controller Design

By neglecting the loss occurring in power semiconductors, one can assume that the average power at the inverter DC side (P_{dc}) is equal to the average power at the AC side (P_{ac}) of the single-phase APF. So, based on Figure 1, we have

$$\frac{1}{T}\int_0^T V_{S,\max} i_{F,\max} \sin^2(\omega t) d\omega t = i_{dc} v_{dc} \tag{8}$$

where $V_{S,max}$ and $i_{F,max}$ are the peak values of the grid voltage (which assumed to be constant) and active fundamental current absorbed by the APF (which is in-phase with the grid voltage), respectively. By simplification, (8) will be

$$-\frac{1}{2} V_{S,\max} i_{F,\max} = C_{dc} \frac{dv_{dc}}{dt} v_{dc} = \frac{1}{2} C_{dc} \frac{dv_{dc}^2}{dt} \tag{9}$$

Applying the small-signal linearization to (9), yields

$$-\frac{1}{2} V_{S,\max} \left(I_{F,\max} + \hat{i}_{F,\max}\right) = \frac{1}{2} C_{dc} \frac{d}{dt} \left(V_{dc}^2 + 2V_{dc}\hat{v}_{dc} + \hat{v}_{dc}^2\right) \tag{10}$$

The DC components of (10) and the second-order perturbations are assumed to be zero. So, the AC components are

$$-\frac{1}{2} V_{S,\max} \hat{i}_{F,\max} = C_{dc} V_{dc} \frac{d\hat{v}_{dc}}{dt} \tag{11}$$

Assuming that the load current has a negligible dynamic behavior, $-i_{F,max}$ can be replaced by $i_{S,max}$. By applying the Laplace operator to (11), the result becomes

$$G_{v_{dc}}(s) = \frac{\hat{v}_{dc}(s)}{\hat{i}_{S,\max}} = \frac{V_{S,\max}}{2C_{dc}V_{dc}s} \tag{12}$$

The closed-loop transfer function of DC-link voltage by noting to Figure 2 is obtained as

$$\frac{v_{dc}(s)}{v_{dc,ref}(s)} = \frac{V_{S,\max}(K_P s + K_I)}{2C_{dc}V_{dc}s^2 + V_{S,\max}(K_P s + K_I)} \tag{13}$$

Tuning the PI controller is a tradeoff between accessible control bandwidth and the loop stability. The effect of the integral part of PI controller around crossover frequency can be neglected. So, (13) without integral gain simplifies to

$$\left.\frac{v_{dc}(s)}{v_{dc,ref}(s)}\right|_{K_I=0} = \frac{V_{S,\max}K_P}{2C_{dc}V_{dc}s + V_{S,\max}K_P} \tag{14}$$

Considering –3dB attenuation of (14) at the DC-link voltage bandwidth frequency, gives the proportional gain of DC-link voltage controller as

$$K_P = \frac{2C_{dc}V_{dc}\omega_v}{V_{S,\max}} \tag{15}$$

The voltage bandwidth frequency is selected below one-tenth the grid voltage frequency. The integral part of the DC-link PI controller is tuned according to the symmetrical optimum (SO) theory. So, K_I is obtained as

$$K_I = \frac{2C_{dc}V_{dc}\omega_v^2}{V_{S,\max}b} \tag{16}$$

where b is a design parameter which determines the system phase margin (PM) as

$$\mathrm{PM} = \tan^{-1}\left(\frac{b^2-1}{2b}\right) \tag{17}$$

Usually, due to digital system and un-modelled delays, the PM is selected above 45°. In this article, we select the PM equal to 70°.

In order to discretize the DC-link voltage controller, used from Backward Euler discretization method. In this method, the integral part of the PI controller is defined as

$$G_{PI}(z) = K_P + K_I \frac{T_{samp} z}{z-1} \tag{18}$$

where T_{samp} is the sampling time of the digital system. Also, the difference equation of the DC-link voltage control which can be used for digital signal controller (DSC) is

$$i_{S,ref\_abs}[k] = i_{S,ref\_abs}[k-1] + (K_P + K_I T_{samp})\big(V_{dc,ref}[k] - V_{dc}[k]\big) \tag{19}$$

where i_{s,ref_abs} is the output signal of the DC-link voltage controller.

3. MULTI-RESONANT CURRENT CONTROL

Resonant controllers are the family of controllers that have a high gain at the reference signal frequency and its multiples. The transfer function of an ideal resonant controller is

$$G_{R,ideal}(s) = \frac{Ks}{s^2 + (n\omega)^2} \tag{20}$$

Figure 3(a) shows the bode diagram of (20) with $K = 20$, $\omega = 100\pi$ rad/s, and $n \in \{1,3,5\}$. As can be seen in this figure, the resonant controller has very high (infinite) gain (above 10^6) with a very low bandwidth. This gain can lead to instability of the controller. So, to overcome on this problem, the nonideal resonant controller is defined as follows

$$G_{R,nonideal}(s) = \frac{Ks}{s^2 + \omega_c s + (n\omega)^2} \tag{21}$$

where ω_c is the bandwidth around the frequency of $n\omega$. Figure 3(b) shows the bode diagram of (21) with $K = 20$, $\omega = 100\pi$ rad/s, $n \in \{1,3,5\}$, and $\omega_c = 10$ rad/s.

It should be noted that the pass-band of each resonant controller is required to be small enough to ensure that each controller responds to the frequencies around its resonant frequency and has a very negligible effect on the stability margin and dynamic performance of the APF.

According to the high-percentage of the lower-order harmonics in the load current and voltage waveforms, only the resonant controllers at the third, fifth, seventh, and ninth orders are used in this article. A resonator at the fundamental frequency is also added to precisely compensate for the reactive fundamental component of the current. The gain K for each of these resonant controllers is selected as $K_h = \{2, 6, 10, 14, 18\} \times \omega$, $k \in \{1, 3, 5, 7, 9\}$. The parameter ω_c is selected to be equal 12 rad/s, which is a compromise between the stability and harmonic rejection capability.

In order to discretize multi-resonant controllers, zero-order hold (ZOH) method which is a suitable discretization technique, is adopted. By this method, the resulted digital resonator will be

$$G_{R,nonideal}(z) = \frac{Ke^{-\frac{\omega_c}{2}T_{samp}} \sin(\omega_1 T_{samp})}{\omega_1} \times \frac{z-1}{z^2 - 2ze^{-\frac{\omega_c}{2}T_{samp}} \cos(\omega_1 T_{samp}) + e^{-\omega_c T_{samp}}} \tag{22}$$

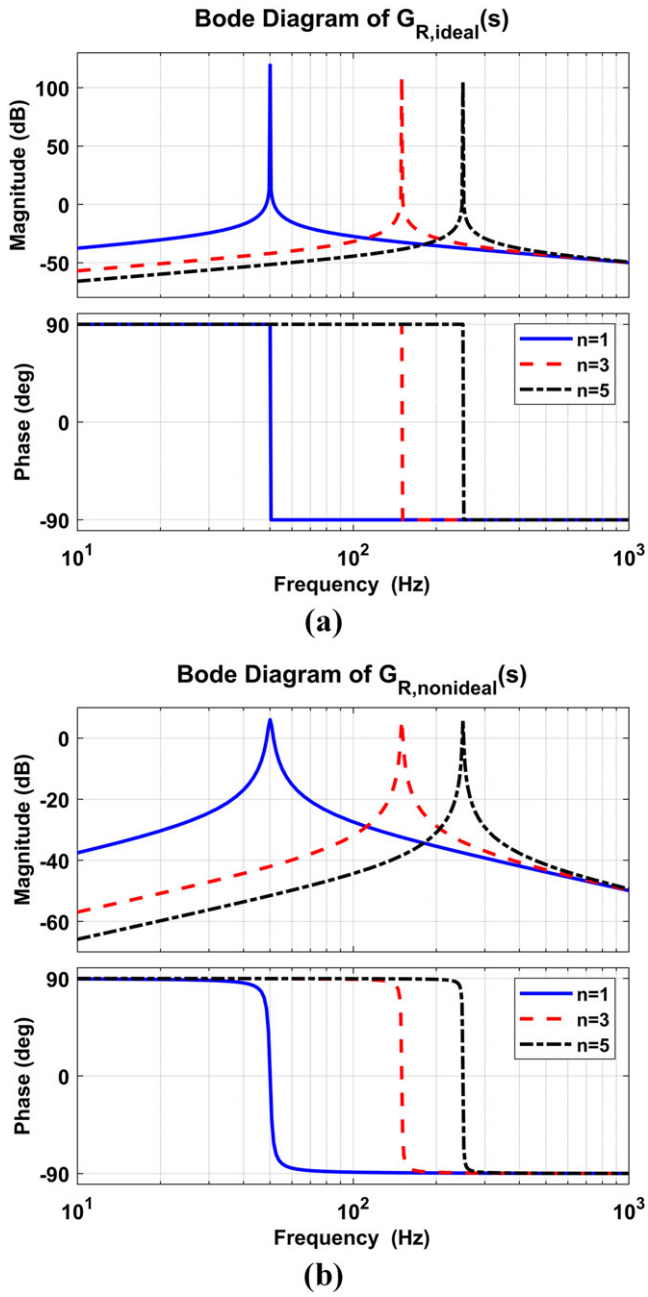

FIGURE 3. Bode diagram of the resonant controller with $K = 20$, $\omega = 100\pi$ and $n \in \{1,3,5\}$; (a) ideal resonator, and (b) nonideal resonator.

where ω_1 is

$$\omega_1 = \sqrt{n^2\omega^2 + \frac{\omega_c^2}{4}} \tag{23}$$

The difference equation of one nonideal resonant controller is

$$\begin{aligned} y_{res}[k] = {} & 2e^{-\frac{\omega_c}{2}T_{samp}} \cos(\omega_1 T_{samp}) y_{res}[k-1] \\ & - e^{-\omega_c T_{samp}} y_{res}[k-2] \\ & + \frac{Ke^{-\frac{\omega_c}{2}T_{samp}} \sin(\omega_1 T_{samp})}{\omega_1} \\ & \times \Big(\big(i_{S,ref}[k-1] - i_S[k-1]\big) \\ & - \big(i_{S,ref}[k-2] - i_S[k-2]\big) \Big) \end{aligned} \tag{24}$$

where y_{res} is the output signal of the resonant controller.

4. SIMULATION AND EXPERIMENTAL RESULTS

In order to confirm theoretical results, simulation and experimental results on a typical system are provided. Simulations are done in MATLAB/Simulink environment. The system parameters are: $v_S = 220\text{V}_{\text{rms}}$, $L = 3\,\text{mH}$, $r_L = 0.5\Omega$, $C_{dc} = 2.2\,\text{mF}$ and $T_{switching} = 0.0001\text{s}$. The experimental setup consisting of DC-link capacitor, a full-bridge IGBT intelligent power module, an inductance filter, measurements and gate drive circuits. The nonlinear load of the setup consists of a single-phase full-bridge diode rectifier feeding a resistor in parallel with a capacitor. The grid voltage and current and the grid current harmonic spectrums are calculated and displayed by the power quality analyzer, Fluke 435. The control algorithm is implemented on a STM32F407VGT6 digital signal controller from the ST. The grid voltage has total harmonic distortion (THD) equal to 5%. Figure 4 shows the simulated grid voltage and current before current compensation. The load current THD is equal to 33%. When single-phase APF is

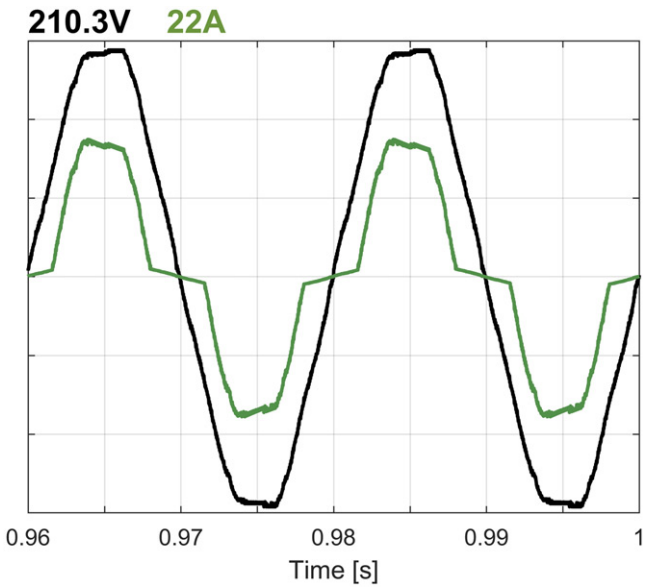

FIGURE 4. Simulated grid voltage (black, 100 V/div) and grid current (green, 20 A/div) before compensation.

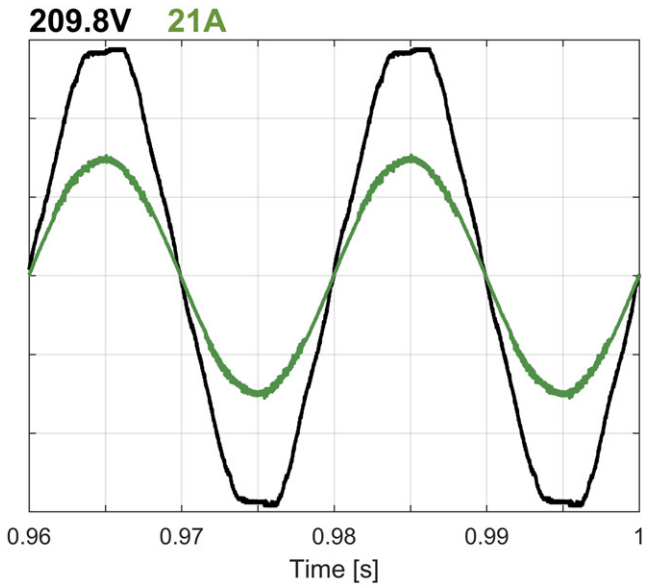

FIGURE 5. Simulated grid voltage (black, 100 V/div) and grid current (green, 20 A/div) after compensation.

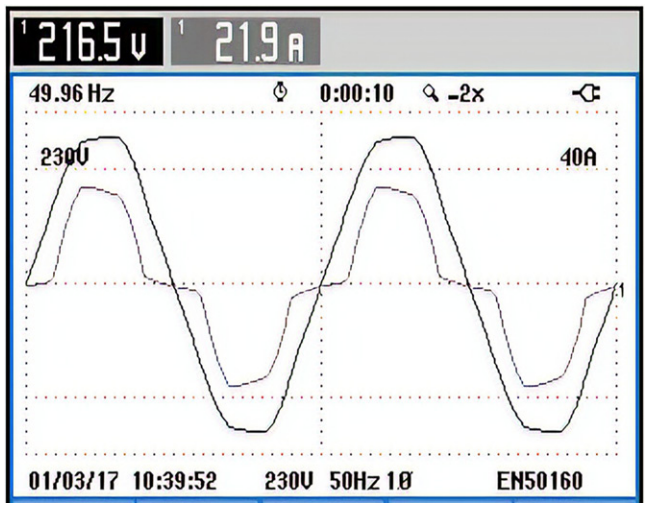

FIGURE 6. Experimental grid voltage and grid current before compensation.

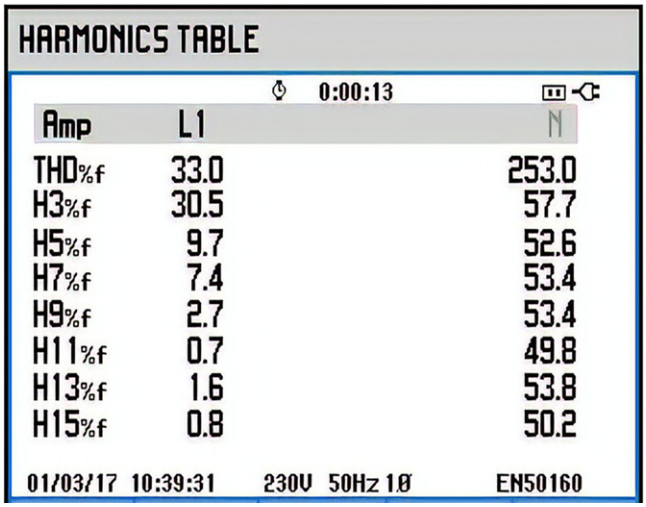

FIGURE 7. Grid current harmonic table before compensation.

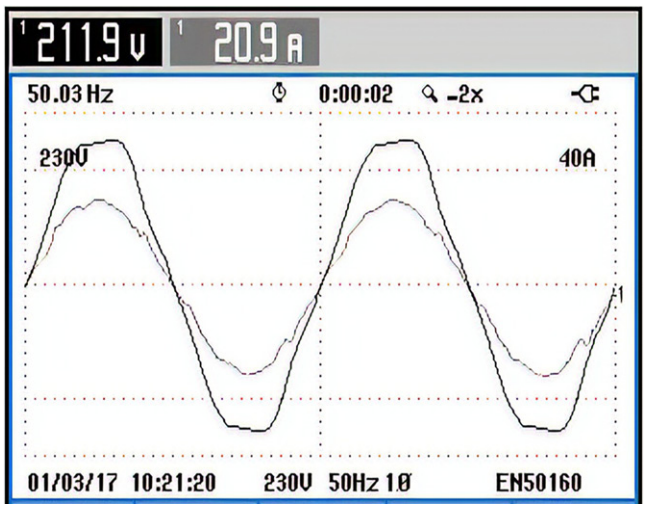

FIGURE 8. Experimental grid voltage and grid current after compensation.

connected to the grid at PCC, the grid current THD decreases to 3.5%. The result is shown in Figure 5. As we can see, the grid current follows the standards limit. Figures 6 and 7 show the experimental grid voltage and current and grid current harmonic table before current compensation, respectively. By connecting APF to the grid, the grid current THD decreases to 4.5% and results are shown in Figures 8 and 9. As shown in these figures, the grid current quality is much improved, the major current harmonics (third, fifth, seventh, and ninth) are well damped, the grid current THD is obtained less than the grid voltage THD and the correct and appropriate performance of the control system is confirmed.

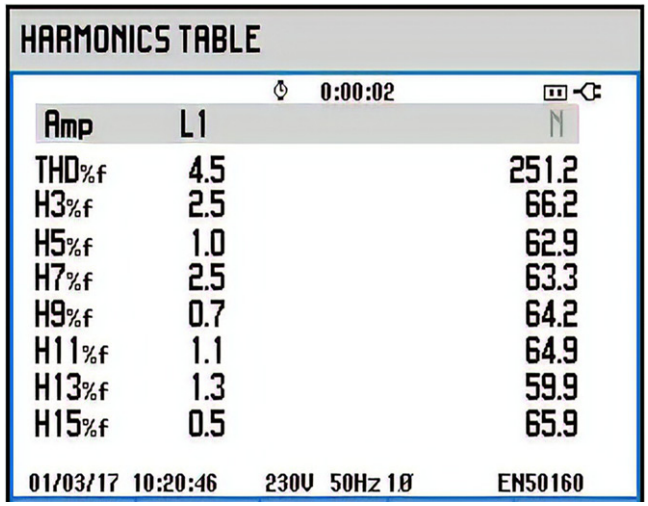

FIGURE 9. Grid current harmonic table after compensation.

5. CONCLUSION

This article proposed a multi-resonant indirect current control method for single-phase shunt APFs. This method has advantages of simplicity, low computational burden and low current ripple. The inner and outer controller design is analyzed in details. Also, the digital representation of the control system is provided to implement on a digital signal controller. Simulation and experimental results on a typical system is provided in this article, also. The results confirm the effectiveness and correct performance of the proposed technique.

REFERENCES

[1] M.-S. Karbasforooshan, and M. Monfared, "An adaptive recursive discrete Fourier transform technique for the reference current generation of single-phase shunt active power filters," in *7th power Electronics and Drive Systems Technologies Conference (PEDSTC)*, 2016, pp. 253–259,

[2] K. Borisov, and H. Ginn, "A computationally efficient RDFT-based reference signal generator for active compensators," *IEEE Trans. Power Deliv.*, vol. 24, no. 4, pp. 2396–2404, Oct. 2009.

[3] J. M. Maza-Ortega, J. A. Rosendo-Macias, A. Gomez-Exposito, S. Ceballos-Mannozzi, and M. Barragan-Villarejo, "Reference current computation for active power filters by running DFT techniques," *IEEE Trans. Power Deliv*, vol. 25, no. 3, pp. 1986–1995, Jul. 2010. DOI: 10.1109/TPWRD.2010.2048764.

[4] V. Khadkikar, A. Chandra, and B. N. Singh, "Generalised single-phase p-q theory for active power filtering: simulation and DSP-based experimental investigation," *IET Power Electron*, vol. 2, no. 1, pp. 67–78, Jan. 2009. DOI: 10.1049/iet-pel:20070375.

[5] M. I. M. Montero, E. R. Cadaval, and F. B. Gonzalez, "Comparison of control strategies for shunt active power filters in three-phase four-wire systems," *IEEE Trans. Power Electron*, vol. 22, no. 1, pp. 229–236, Jan. 2007. DOI: 10.1109/TPEL.2006.886616.

[6] M.-S. Karbasforooshan, and M. Monfared, "Design and implementation of a single-phase shunt active power filter based on PQ theory for current harmonic compensation in electric distribution networks," in *IECON 2017 – 43rd Annual Conference of the IEEE Industrial Electronics Society*, 2017, pp. 6389–6394

[7] M. Monafred, S. Golestan, and J. M. Guerrero, "A new synchronous reference frame-based method for single-phase shunt active power filters," *J. Power Electron.,* vol. 13, no. 4, pp. 692–700, Jul. 2013. DOI: 10.6113/JPE.2013.13.4.692.

[8] A. Fereidouni, and M. A. S. Masoum, "Shunt active power filter enhancement by means of frequency-locking complex adaptive linear combiner," *Electr. Power Components Syst.*, vol. 44, no. 20, pp. 2256–2270, Dec. 2016. DOI: 10.1080/15325008.2016.1220997.

[9] C. Siluvaimuthu, and V. Chenniyappan, "A low-cost reconfigurable field-programmable gate array based three-phase shunt active power filter for current harmonic elimination and power factor constraints," *Electr. Power Components Sys.t*, vol. 42, no. 16, pp. 1811–1826, Dec. 2014. DOI: 10.1080/15325008.2014.949911.

[10] P. Matavelli, and F. P. Marafao, "Repetitive-based control for selective harmonic compensation in active power filters," *IEEE Trans. Ind. Electron*, vol. 51, no. 5, pp. 1018–1024, Oct. 2004. DOI: 10.1109/TIE.2004.834961.

[11] R. Costa-Castello, R. Grino, and E. Fossas, "Odd-harmonic digital repetitive control of a single-phase current active filter," *IEEE Trans. Power Electron*, vol. 19, no. 4, pp. 1060–1068, 2004. Jul. DOI: 10.1109/TPEL.2004.830045.

[12] A. Ghamri, M. T. Benchouia, and A. Golea, "Sliding-mode control based three-phase shunt active power filter: simulation and experimentation," *Electr. Power Components Syst.*, vol. 40, no. 4, pp. 383–398, Jan. 2012. DOI: 10.1080/15325008.2011.639127.

[13] R. Panigrahi, P. C. Panda, and B. Subudhi, "A robust extended complex Kalman filter and sliding-mode control based shunt active power filter," *Electr. Power Components Syst.*, vol. 42, no. 5, pp. 520–532, Apr. 2014. DOI: 10.1080/15325008.2013.871609.

[14] T. Al Chaer, L. Rambault, J.-P. Gaubert, C. Dewez, and M. Najjar, "H∞ static control law for a three-phase shunt active power filter," *Electr. Power Components Syst.*, vol. 36, no. 2, pp. 152–169, Jan. 2008. DOI: 10.1080/15325000701549160.

[15] X. Tang, K. M. Tsang, and W. L. Chan, "Active power filter using nonlinear repetitive controller," *Int. J. Control. Autom. Syst.*, vol. 9, no. 1, pp. 132–138, Feb. 2011. DOI: 10.1007/s12555-011-0117-3.

[16] M. Qasim, P. Kanjiya, and V. Khadkikar, "Artificial-neural-network-based phase-locking scheme for active power filters," *IEEE Trans. Ind. Electron*, vol. 61, no. 8, pp. 3857–3866, 2014. Aug. DOI: 10.1109/TIE.2013.2284132.

[17] L. Saribulut, A. Teke, and M. Tumay, "Artificial neural network-based discrete-fuzzy logic controlled active power filter," *IET Power Electron*, vol. 7, no. 6, pp. 1536–1546, Jun. 2014. DOI: 10.1049/iet-pel.2013.0522.

[18] T. Narongrit, K. Areerak, and K. Areerak, "A new design approach of fuzzy controller for shunt active power filter," *Electr. Power Components Syst.*, vol. 43, no. 6, pp. 685–694, Apr. 2015. DOI: 10.1080/15325008.2014.996680.

[19] D. Suresh, and S. P. Singh, "Type-2 fuzzy logic controlled three-level shunt active power filter for power quality improvement," *Electr. Power Components Syst.*, vol. 44, no. 8, pp. 873–882, May 2016. DOI: 10.1080/15325008.2016.1138158.

[20] T. Narongrit, K. Areerak, and K. Areerak, "Adaptive fuzzy control for shunt active power filters," *Electr. Power Components Sys.t*, vol. 44, no. 6, pp. 646–657, Apr. 2016 DOI: 10.1080/15325008.2015.1122111.

[21] M.-S. Karbasforooshan, M. Monfared, and M. Dogruel, "Indirect control of single-phase active power filters using harmonic control arrays," in *2017 Electrical Power Distribution Networks Conference (EPDC)*, 2017, pp. 143–148.

BIOGRAPHIES

Mohammad-Sadegh Karbasforooshan received the B.Sc. and the M.Sc. degrees (both with honors) in electrical engineering from Ferdowsi University of Mashhad, Iran, in 2013, and 2015. He is currently working toward the Ph.D. degree at Ferdowsi University of Mashhad, Iran. His research interests include power electronics, active power filters, and power quality.

Mohammad Monfared received the B.Sc. degree in electrical engineering from Ferdowsi University of Mashhad, Iran, in 2004, and the M.Sc. and Ph.D. degrees (both with honors) in electrical engineering from Amirkabir University of Technology, Tehran, Iran, in 2006 and 2010. He is currently an Associate Professor at Ferdowsi University of Mashhad, Iran, where he has received the Best Researcher Award in 2015. His research interests include power electronics, renewable energy systems, and power quality.